Available online at www.sciencedirect.com
SCIENCE DIRECT®
Journal of Power Sources 140 (2005) 81–87
JOURNAL OF POWER SOURCES
www.elsevier.com/locate/jpowsour

Porous nickel MCFC cathode coated by potentiostatically deposited cobalt oxide
I. A structural and morphological study

M.J. Escudero[a,*], T. Rodrigo[b], L. Mendoza[c], M. Cassir[c], L. Daza[a,b]

[a] *Environment and Technology Research Centre (CIEMAT), Fossil Fuel department, Av. Complutense 22, 28040 Madrid, Spain*
[b] *Institute of Catalysis and Petrochemistry (CSIC), Campus Cantoblanco 28049, Spain*
[c] *Ecole Nationale Supérieure de Chimie de Paris (ENSCP), Laboratoire d'Electrochimie et de Chimie Analytique (UMR 7575 du CNRS), 11 rue Pierre et Marie Curie, 75231 Paris Cedex 05, France*

Received 4 March 2004; received in revised form 17 July 2004; accepted 16 August 2004
Available online 6 October 2004

Abstract

Porous nickel cathode was protected by potentiostatically deposited cobalt at different experimental conditions: oxidation potential and electrolysis duration. The deposition growth increased with the oxidation potential yielding a more developed granular structure with smaller grains. Thin layers of Co_3O_4 were identified by X-ray diffraction (XRD) and Raman spectroscopy. CoOOH was detected by X-ray photoelectron spectroscopy (XPS) before annealing treatment and Co_3O_4 after heating the sample at 500 °C during 4 h in air. After this treatment, some morphological changes were observed on the coated samples due to grain compaction and oxidation of the nickel substrate. The porosity of the coated samples was relatively close to that of the sole porous nickel. These coatings exhibited an appropriate dual-pore structure with macro and micro pores, a basic MCFC requirement.

Keywords: Co_3O_4 coating; Porous nickel cathode; Molten carbonate; Fuel cell; XRD; Raman spectroscopy; XPS; Porosity

1. Introduction

The interest of $LiCoO_2$ as a candidate material for replacing the state-of-the-art molten carbonate fuel cell (MCFC) cathode, $Li_xNi_{1-x}O$, is well described in the literature [1–6]. This compound is less soluble than the nickel cathode in the MCFC conditions and has an electrocatalytical activity close to that of $Li_xNi_{1-x}O$. However, its conductivity is lower than that of the usual cathode material, its mechanical resistance is lower and its cost is relatively high. In addition, problems in scale up of electrode area restrict its use. The thin layer technology is an interesting way of solving these practical problems by combining the properties of the $LiCoO_2$ coating (low solubility) and the $Li_xNi_{1-x}O$ substrate (cheap, good conductivity and mechanical strength). The feasibility of coating the nickel cathode with well-controlled $LiCoO_2$ thin layers has been analysed in recent papers [7–10].

In a previous work, we have developed and optimised the electrochemical deposition of Co_3O_4 thin layers on dense nickel or nickel oxide substrates [11,12]. This cheap and room-temperature technique allowed us to obtain thin and homogeneous layers of Co_3O_4 transformed into $LiCoO_2$ after exposure to the molten carbonate melt. The use of dense nickel or nickel oxide substrates was a first necessary step to analyse thoroughly the structural and morphological features of the cobalt coatings; nevertheless, the situation can be significantly different in the case of porous electrodes. The present paper is dedicated to the elaboration and characterisation of cobalt oxide deposits on the porous nickel cathode before its oxidation and lithiation in situ in molten Li_2CO_3–Na_2CO_3, one of the

* Corresponding author. Tel.: +34 91 3466 622; fax: +34 91 3466 269.
E-mail address: m.escudero@ciemat.es (M.J. Escudero).

0378-7753/$ – see front matter © 2004 Elsevier B.V. All rights reserved.
doi:10.1016/j.jpowsour.2004.08.009

Table 1
Name and description of all the samples analyzed in the present study

Sample	E/V vs. Hg/Hg_2Cl_2	Electrolysis time (h)	Annealing treatment
Ni			No
NiCo0.50t8	0.50	8	No
NiCo0.65t8	0.65	8	No
NiCo0.50t24	0.50	24	No
NiCo0.65t24	0.65	24	No
NiO			Yes
NiOCo0.50t8	0.50	8	Yes
NiOCo0.65t8	0.65	8	Yes
NiOCo0.50t24	0.50	24	Yes
NiOCo0.65t24	0.65	24	Yes

candidate electrolytes for MCFC application, in the standard conditions. The structural properties of the deposits were characterised either directly or after an annealing treatment by X-ray diffraction (XRD), Raman spectroscopy, X-ray photoelectron spectroscopy (XPS). The morphological features were analysed by scanning electron microscopy (SEM) associated with energy-dispersive spectroscopy (EDS) and the pore size deposition by mercury porosimetry.

2. Experimental

2.1. Electrochemical deposition

The samples were prepared by potentiostatic deposition of cobalt oxide films on porous Ni foils (6 mm × 25 mm × 0.5 mm). The deposition was performed in a four-compartment Tacussel glass cell with a 0.1 mol l^{-1} Co(II) solution prepared from $Co(NO_3)_2{\cdot}6H_2O$ (Fluka, with a purity of 99.99% analytical-reagent grade chemical) in a 0.5 mol l^{-1} solution of $NaNO_3$ (Merck) with a pH = 4. The solution was de-aerated during 30 min prior to electrochemical deposition and the pH fixed at 7.4 by addition of a 1 mol l^{-1} NaOH solution. The working electrode was a porous nickel foil, the counter electrode was a Pt foil and the reference electrode was a $Hg|Hg_2Cl_2$ (SCE) which was placed in a separate compartment filled with a 0.5 mol l^{-1} $NaNO_3$. The potentiostatic deposition was performed by means of a Princeton Applied Research (PAR) Model 263 system. The effect of two different potentials 0.50 and 0.65 V versus SCE, at two different electrolysis durations 8 and 24 h, before and after thermal treatment (at 500 °C during 4 h in air at a heating rate of 1 °C min^{-1}), on the cobalt oxide deposits, was investigated. All the samples studied in this work are reported in Table 1.

2.2. Characterisation techniques

XRD analyses were performed with a Philips Model X′Pert-MPD diffractometter using a Cu Kα radiation (λ = 1.542 Å). The diffraction intensity was measured in the 2°–90° (2θ) range, by steps of 0.05° (2θ) with a counting time of 2 s.

Raman spectra were obtained at room temperature with a Bruker RFS-100 FT-Raman spectrometer provided with a diode-pumped germanium solid-state detector, which operates at liquid N_2 temperature. An Nd:YAG laser was used as exciting source. The samples were pressed into the holder with no other pre-treatment. A laser power of ca. 600 mW was used, the spectra being taken with a resolution 4 cm^{-1} and accumulating 500 scans. For each measurement the integration time was 30 min.

XPS analysis was performed with a Perkin-Elmer PHI 5400 spectrometer equipped with a Mg Kα excitation source (hν = 1253.60 eV) and a beam size of 1 mm diameter. Typical operation conditions were: X-ray gun, 15 kV, 20 mA, pressure in the sample chamber $\sim 10^{-9}$ Torr, pass energy, 89.50 eV for general spectra (0–1100 eV) and 35.75 eV for high resolution spectra. In order to take into account the charging effects on the measured binding energies, these energies were determined by referencing to the C 1s peak at 284.8 eV.

The morphology and composition of the deposits were examined with SEM using a Hitachi microscope S-2500 combined with EDS, model Sun Sparcstation.

The porosity and the pore size distribution were determined by mercury porosimetry using a Micrometrics Pore Sizer 9310.

3. Results and discussion

Fig. 1 shows the XRD patterns of the cobalt oxide formed on the porous nickel foil obtained at 0.65 V during 24 h, before and after the thermal treatment (4 h at 500 °C in air). Initially, only the XRD peaks corresponding to metallic nickel were observed at 44.50°, 51.84°, and 76.37°(2θ). After the annealing treatment, apart of the XRD peaks of Ni, less intense peaks were detected: they correspond to NiO at 37.28°, 42.23°, and 62.97° (2θ) and to cubic Co_3O_4 compound that appear at 19.00°, 31.27°, 36.85°, 59.35°, and 65.23° (2θ). This indicates that the formation of cubic Co_3O_4 on porous Ni is only obtained after an annealing process. A similar behaviour was obtained for all the other samples, but the intensity of the peaks relative cubic Co_3O_4 decreases with reducing both potential and electrolysis duration. However, it is difficult to obtain a detailed information about the crystallographic structure of deposits because the cobalt content is much lower than that of nickel.

Raman spectroscopy is a tool providing information on the vibrations of atoms in crystals and is very sensitive to the symmetry of crystallographic structures. The Raman spectra of the samples with cobalt deposits on porous nickel, before and after annealing treatment, are presented in Fig. 2. Initially, these samples showed two broad bands around 501 and 613 cm^{-1} that did not appear in the porous nickel Raman spectrum. This suggests that theses bands are due to the presence of cobalt on the porous substrate. The intensity of these bands increased with the imposed potential and the electrolysis duration and, therefore, with the cobalt content,

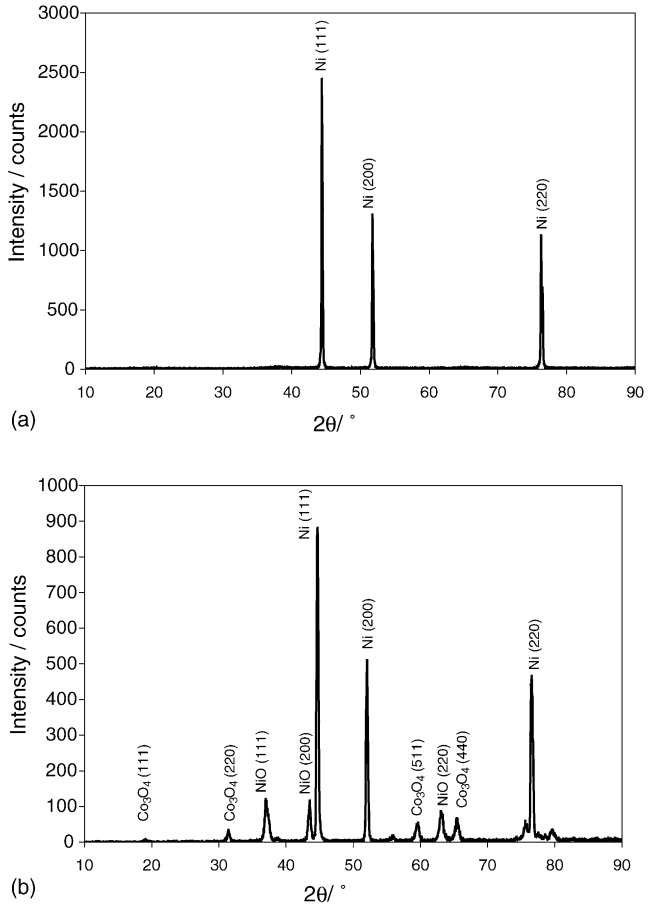

Fig. 1. XRD patterns: (a) NiCo0.65t24, (b) NiOCo0.65t24.

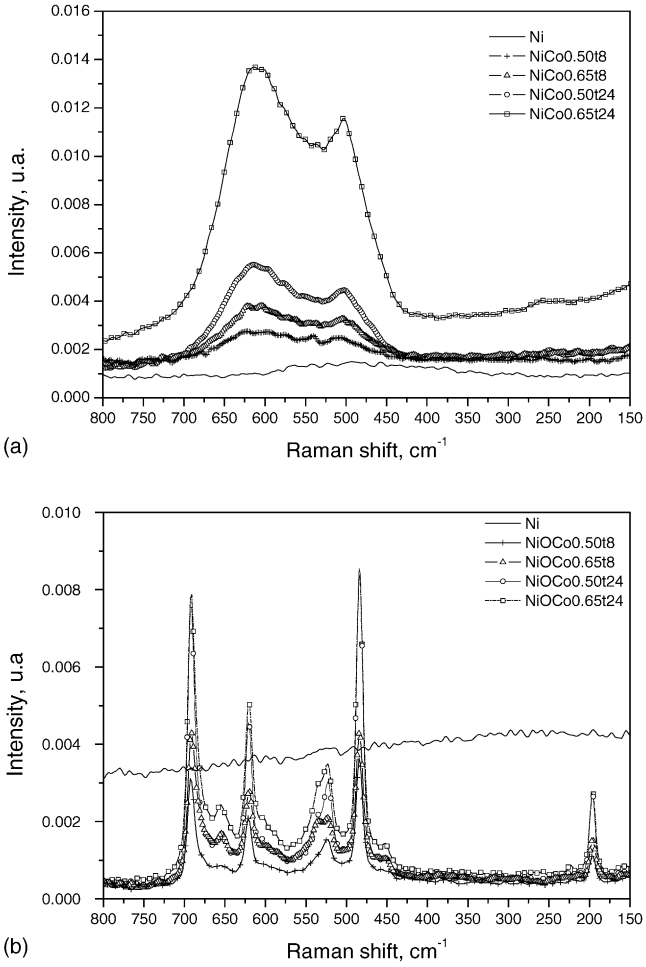

Fig. 2. Raman spectra of porous Ni and cobalt deposits on nickel porous: (a) before heat treatment, (b) after heat treatment.

as can be seen in Table 2 (comments will be given forward). After the heat treatment, five bands, not present in the porous nickel spectrum, were observed at 197, 484, 523, 621, and 691 cm^{-1}. Co_3O_4 crystallizes in the normal spinel structure Co^{2+} $(Co^{3+})_2O_4{}^{2-}$ and belongs to the space group $O^7{}_h$-Fd 3m. The spinel lattice is constituted of Co^{2+} and Co^{3+} located at tetrahedral and octahedral sites, respectively. The active vibrations of spinel structure (Fd 3m) are $A_{1g} + E_g + F_{1g} + 3F_{2g} + 2A_{2u} + 2E_u + 4F_{1u} + 2F_{2u}$. The A_{1g}, E_g, and $3F_{2g}$ modes are Raman active, and $4F_{1u}$ are infrared active. The reaming F_{1g}, $2A_{2u}$, $2E_u$, and $2F_{2u}$ modes are inactive [13,14]. Therefore, five Raman bands observed for the samples (Fig. 2b) can be assigned to Raman active or phonon modes of Co_3O_4: the peaks at 197, 523, and 621 cm^{-1} corresponds to F_{2g} phonon modes whereas the peaks at 484 and 691 cm^{-1} are E_g and A_{1g} phonon modes [13,15]. The phonon symmetries determined in this work are in agreement with those given by Hadjiev et al. [13] and Herrera and Resasco [15]. Therefore, this confirms that the crystallographic structure of the deposits, after an annealing treatment, corresponds to Co_3O_4.

Table 2
Chemical composition of coated samples (relative percentage of Ni and Co) without or with annealing treatment determined by energy-dispersive spectroscopy (EDS)

Sample	Ni atomic (%)	Co atomic (%)
Ni	–	–
NiCo0.50t8	75.36	24.56
NiCo0.65t8	59.72	40.18
NiCo0.50t24	40.27	59.63
NiCo0.65t24	22.11	77.82
NiO	–	–
NiOCo0.50t8	87.69	12.27
NiOCo0.65t8	73.31	26.61
NiOCo0.50t24	56.78	43.12
NiOCo0.65t24	29.44	70.48

XPS spectra can provide information on the qualitative analysis of cobalt oxide deposits and on the identification of the valence state of cobalt in order to determine the effect of the imposed potential, the electrolysis time and the heat treatment on the crystallographic structure of deposits. The survey spectrum of each deposit on porous nickel revealed the presence of Co, O, Ni and C in the surface (also confirmed by the Auger lines). Nickel was detected for all the deposits and the cobalt content increased at higher deposition voltage and higher electrolysis duration.

Table 3
XPS BEs of Co $2p_{3/2}$ and O 1s peaks of the coated samples without or with annealing treatment

Sample	Co 2p3/2 BE (eV)	Δ_1 (eV)	Δ_2 (eV)	O 1s BE (eV)
NiCo0.50t8	781.2	15.9	–	528.6 (O_I;3%); 531.1 (O_{II};78%); 532.7 (O_{III};19%)
NiCo0.65t8	780.6	15.7	–	529.4 (O_I;21%); 533.4 (O_{II};74%); 532.5 (O_{III};5%)
NiCo0.50t24	780.4	15.9	–	529.2 (O_I;6%); 531.0 (O_{II};70%); 532.7 (O_{III};24%)
NiCo0.65t24	780.2	15.2	–	529.6 (O_I;21%); 531.2 (O_{II};71%); 533.3 (O_{III};8%)
NiOCo0.50t8	779.8	15.0	9.5	529.6 (O_I;49%); 531.2 (O_{II};42%); 532.8 (O_{III};9%)
NiOCo0.65t8	779.8	15.0	9.8	529.6 (O_I;49%); 531.2 (O_{II};42%); 532.8 (O_{III};9%)
NiOCo0.50t24	779.7	15.2	9.9	529.2 (O_I;52%); 531.0 (O_{II};35%); 532.7 (O_{III};13%)
NiOCo0.65t24	779.8	14.9	9.6	529.6 (O_I;58%); 531.2 (O_{II};35%); 533.3 (O_{III};7%)

The binding energies (BEs) relative to Co $2p_{3/2}$, Δ_1 (Co $2p_{3/2}$-Co $2p_{1/2}$ peak splitting), Δ_2 (peak separation between the Co $2p_{3/2}$ main peak and satellite) and the binding energies values of O 1s for all the deposits are presented in the Table 3. Curve fitting of O 1s signal, gives generally three contributions, which on the basis of their BEs were assigned to oxide lattice (O_I), hydroxyl groups and/or non-stoichiometric surface oxygen (O_{II}), and molecular water adsorbed in the surface(O_{III}), respectively.

XPS data of Co 2p for all the deposits, before and after heat treatment, are presented in Fig. 3. According to the literature, the Co $2p_{3/2}$ spectrum shows a complex structure broadened by multiplet splitting effects and, in addition, very similar binding energies are known for most of the cobalt oxides and hydroxides (i.e. CoO, Co_2O_3, Co_3O_4, CoOOH) [12,15–18]. However, a detailed analysis of the Co 2p shake-up structure should allow the assignment of cobalt oxidation states. In fact, it is well known that all the Co^{2+} compounds are high spin complexes with strong satellite bands, while all the Co^{3+} are diamagnetic [17,18].

Before the annealing treatment, the BEs values of Co 2p peaks (Table 3) and the absence of the intense satellite bands associated to Co 2p (Fig. 3a) most probably correspond to the presence of CoOOH instead of $Co(OH)_2$. The Co $2p_{3/2}$ and O 1s BEs values for all the samples are in good agreement with the values obtained by McIntyre and Cook [17] and Galtayries and Grimblot [19] for CoOOH.

After the annealing treatment, the cobalt XPS spectra show a higher resolution (Fig. 3b). The Co $2p_{3/2}$ and Co $2p_{1/2}$ peaks are slightly shifted towards lower binding energies values and the Co $2p_{3/2}$ line is narrower. A very weak satellite band, appearing at 9.7 ± 0.2 eV higher than the main peak, are probably due to shake-up effects related to paramagnetic divalent high-spin cobalt [20]. These results and the absence of a strong shake-up satellite structure indicate the presence of Co_3O_4. Similar results were reported for Co_3O_4 by Milton et al. [16] and Casella and Guascito [18].

As shown in Table 3, for all the samples before heat treatment, the contribution of O $1s_{II}$ associated with OH^- groups is the most important contributions between 70 and 78%. However, the contribution of O $1s_I$ is more important for the samples prepared at a potential of 0.65 V versus SCE with respect to those obtained at a potential 0.50 V versus SCE. This indicates that oxide species represent around 21% for NiCo0.65t8 and NiCo0.65t24, while the proportion decreases to 3 and 6% for NiCo0.50t8 and NiCo0.50t24, respectively. This suggests that the deposits obtained at 0.65 V versus SCE present a lower free surface to adsorb water molecules.

After the annealing treatment, the O 1s region for all the deposits present important changes. The main peak corresponds to the lower binding energy ascribed to oxygen species. The second one in importance is assigned to hy-

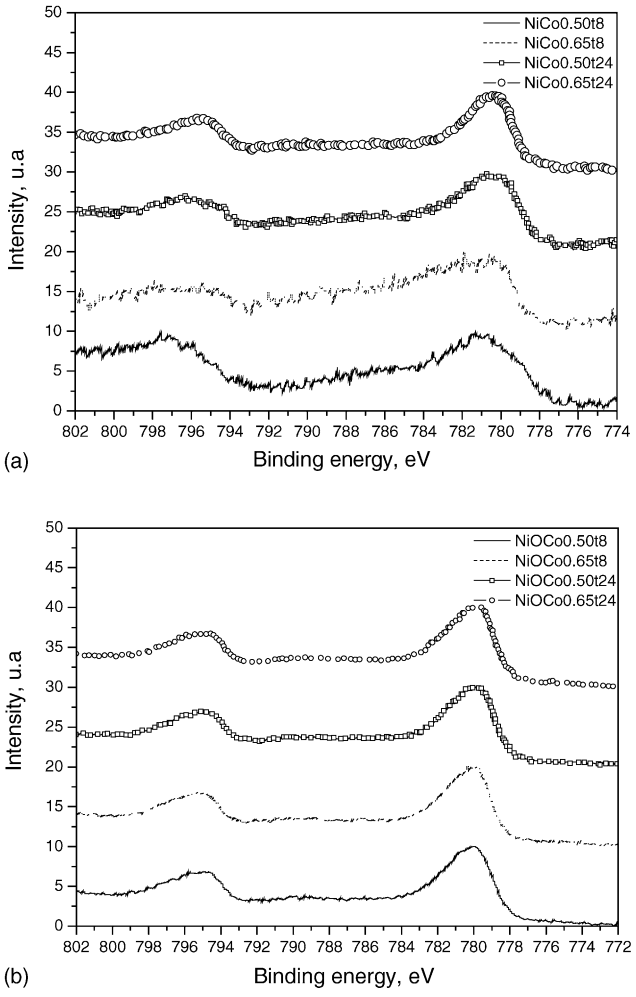

Fig. 3. Co 2p XPS spectra of cobalt deposits on nickel porous: (a) before heat treatment, (b) after heat treatment.

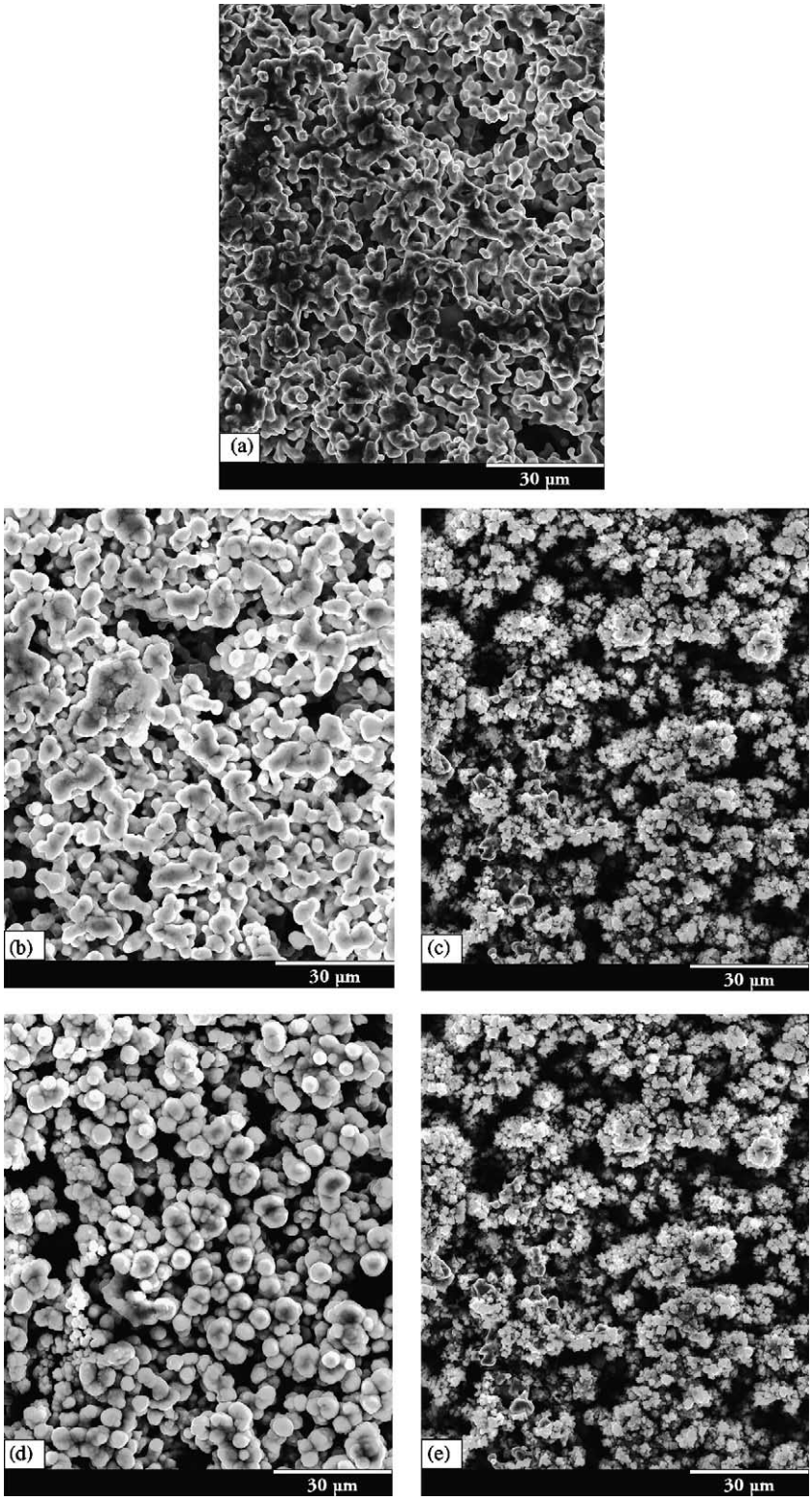

Fig. 4. SEM micrographs: (a) porous Ni, (b) NiCo0.50t8, (c) NiCo0.65t8, (d) NiCo0.50t24, (e) NiCo0.65t24.

droxide species. Therefore, after the annealing treatment, the amount of oxide species is larger than that of hydroxide species (Table 3), suggesting, at least, the partial transformation of CoOOH into Co_3O_4.

These results could be explained assuming that the oxidation reaction of the potentiostatic deposition is:

$$Co(OH)_2 + OH^- \rightarrow CoOOH + 1e^-$$

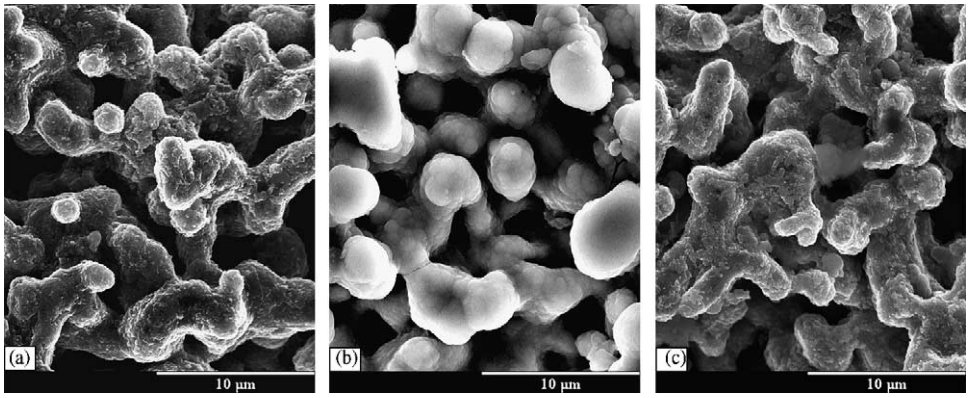

Fig. 5. SEM micrographs: (a) porous NiO, (b) NiCo0.50t8, (c) NiOCo0.50t8.

After thermal treatment, in accordance with Avramon [21], the CoOOH decomposition can be represented as follows:

$$12\mathrm{CoOOH} \rightarrow 4\mathrm{Co_3O_4} + 6\mathrm{H_2O} + 2e^-$$

After the annealing process, no significant difference in the composition of the deposits was observed whatever the imposed potential or the electrolysis duration.

The proportion of nickel with respect to cobalt, determined by EDS, is presented in Table 2, before and after annealing treatment. EDS analysis confirms that the Co content increases at higher deposition potential and electrolysis duration. After the thermal annealing, a loss of cobalt was detected.

SEM micrographs of the Co-coated porous nickel substrates, obtained at two potentials (0.50 and 0.65 V versus SCE) and two deposition durations, 8 and 24 h, before annealing treatment are presented in Fig. 4. From these micrographs, it can be deduced that the morphology of coated porous nickel cathodes presents a granular structure, more developed at higher deposition potential (0.65 V versus SCE), and that the grains size decreases at higher deposition potential, which is probably due to a higher deposition velocity.

After the annealing treatment, some morphological changes were observed, most probably due to the cobalt loss, grain compaction and the oxidation of the porous nickel substrate. For example, after the annealing treatment, the morphology of NiCo0.5t8 sample became relatively close to that of NiO as a result of the important cobalt loss, as can be seen in Fig. 5.

The cumulative pore volume and the porosimetry data relative to porous nickel substrate (Ni or NiO, when previously oxidised) and the cobalt oxide coatings on porous nickel, before and after heat treatment, are given in Fig. 6. All the samples exhibit an appropriate dual-pore structure with macro pores (>1 μm) and micro pores (<1 μm). This dual pore structure is a basic requirement for a MCFC cathode: the macro pores serve as gas channels for the fuel cell and the micro pores absorb molten electrolyte by capillary effects. Thus, the MCFC reduction reaction occurs in a ternary phase between the solid cathode phase, the molten electrolyte phase and the gas phase. Initially, all the Ni-Co samples show similar pore distributions, lower than that of nickel (Fig. 6a). After being oxidised in air at 500 °C for 4 h, a reduction of the pore volume distribution was observed for all the samples. This may be due to the decrease in the average inter particle distance when decreasing the porosity. Table 4 shows the porosity and the average pore diameter for all the samples. Initially, the porosity of the coated samples was between 63 and 68%. These porosity values were lower than that of the pure nickel cathode (73%). The thermal treatment reduced the porosity

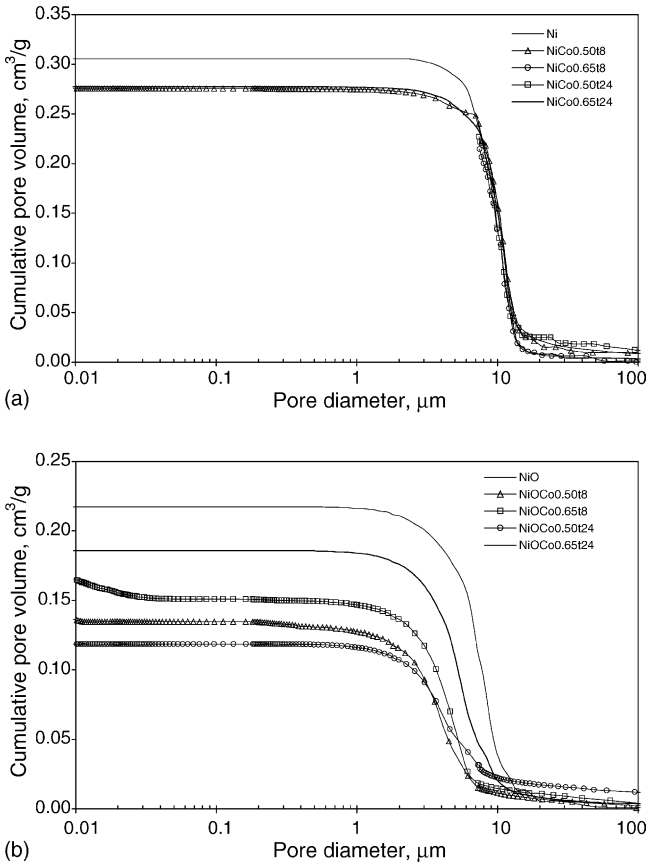

Fig. 6. Pore volume distribution of porous Ni and cobalt deposits on nickel porous: (a) before heat treatment, (b) after heat treatment.

Table 4
Porosity and medium pore diameter of porous nickel and the coated samples without or with annealing treatment

Sample	Porosity (%)	Medium pore diameter (μm)
Ni	73	9.80
NiCo0.50t8	69	10.11
NiCo0.65t8	63	10.43
NiCo0.50t24	64	10.50
NiCo0.65t24	68	9.84
NiO	59	7.16
NiOCo0.50t8	53	3.35
NiOCo0.65t8	48	3.92
NiOCo0.50t24	58	5.54
NiOCo0.65t24	60	4.51

(12–25%) for all the samples. Initially, the particle size was about 10 μm; after the thermal treatment, the pore size decreased to 7.1 μm for porous nickel, and to 3–6 μm for the coated samples. This behaviour may be due to a reduction of grain size and particle compaction produced by the annealing treatment.

4. Conclusion

Cobalt oxide potentiostatic deposition was adapted to the protection of the porous MCFC nickel cathode. After an annealing treatment, provoking a relative loss of the cobalt content, experimental evidence was given on the formation of electrodeposited Co_3O_4 by XRD and Raman spectroscopy. Before the thermal treatment, XPS allowed the detection of CoOOH, which was transformed into Co_3O_4 after annealing. The morphology and porosity of Co_3O_4-coated nickel was relatively close to that of sole porous nickel, showing an appropriate dual pore structure. The annealing treatment provoked a significant reduction of the coated sample grain size. It can be concluded from this study that potentiostatic deposition seems to be very promising: it is a low-cost technique, producing homogeneous layers and adapted to MCFC application. The behaviour of these coatings will be studied in molten carbonates in a forthcoming paper.

References

[1] T. Fukui, H. Okawa, T. Tsunooka, Solubility and deposition of $LiCoO_2$ in a molten carbonate, J. Power Sources 71 (1998) 239–243.
[2] K.-I. Ota, Y. Takeishi, S. Shibata, H. Yoshikate, N. Kamiya, Solubility of cobalt oxide in molten carbonate, J. Electrochem. Soc. 142 (10) (1995) 3322–3326.
[3] R.C. Makkus, K. Hemmes, J.H.W. de Wit, A comparative study of NiO(Li), $LiFeO_2$, and $LiCoO_2$ porous cathodes for moltan carbonate fuel cells, J. Electrochem. Soc. 141 (12) (1994) 3428–3429.
[4] K. Janowitz, M. Kah, H. Wendt, Molten carbonate fuel cell research. Part I. Comparing cathodic oxygen reduction in lithium/potassium and lithium/sodium carbonate melts, Electrochim. Acta 45 (1999) 1025–1037.
[5] L. Giorgi, M. Carewsca, M. Patriarca, S. Scaccia, E. Simmonetti, A. Di Bartolemeo, Development and characterization of novel cathode materials for molten carbonate fuel cell, J. Power Sources 49 (1994) 227–243.
[6] L. Giorgi, M. Carewsca, M. Patriarca, S. Scaccia, E. Simmonetti, E. Giacometti, R. Tulli, Development of molten carbonate fuel cell using novel cathode material, Int. J. Hyd. Energy 21 (1996) 491–496.
[7] S.W. Nam, S.G. Kim, I.H. Oh, T.H. Lim, H.Y. Ha, S.A. Hong, K. Kim, H.C. Lim, 1999, Carbonate fuel cell technology V, in: I. Uchida, et al. (Eds.), $LiCoO_2$-coated NiO cathode for MCFC, PV 99-20, The Electrochemical Society Series, Pennington, NJ, p. 253.
[8] T. Fukui, S. Ohara, H. Okawa, T. Hotta, M. Naito, Properties of NiO cathode coated with lithiated Co and Ni solid solution for MCFCs, J. Power Sources 86 (2000) 340–346.
[9] S.T. Kuk, Y.S. Song, K. Kim, Properties of a new type of cathode for molten carbonate fuel cells, J. Power Sources 83 (1999) 50–56.
[10] S.T. Kuk, Y.S. Song, S.I. Suh, J.Y. Kim, K. Kim, The formation of $LiCoO_2$ on a NiO cathode for a molten carbonate fuel cell using electroplating, J. Mater. Chem. 11 (2001) 630–635.
[11] L. Mendoza, V. Albin, M. Cassir, A. Galtayries, Electrochemical deposition of Co_3O_4 thin layers in order to protct the nickel-based molten carbonate fuel cell cathode, J. Electroanal. Chem. 548 (2003) 95–107.
[12] L. Mendoza, A. Galtayries, A. Ringuedé, M. Cassir, II. Structural, morphological, chemical and electrochemical analysis of nickel covered by electrochemically deposited Co_3O_4 in molten Li_2CO_3-Na_2CO_3 at 650 °C, J. Electroanal. Chem. (2003), in press.
[13] V.G. Hadjiev, M.N. Iliev, I.V. Vergilov, The Raman spectra of Co_3O_4, J. Phys. C: Solid State Phys. 21 (1988) L199–201.
[14] H. Shirai, Y. Moriopka, I. Nakagawa, Infrared and Raman spectra and lattice vibrations of some oxide spinels, J. Phys. Soc. (Japan) 512 (1982) 592–597.
[15] J.E. Herrera, D.E. Resasco, Role of Co-W interaction in the selective growth of single walled carbon nanotubes from CO disproportionation, J. Phys. Chem. B 107 (2003) 3738–3746.
[16] D.B. Mitton, J. Walton, G.E. Thompson, An XPS and AES study of the ageing of a Co-20% Ni metal-evaporated tape, Surf. Interface Anal. 20 (1993) 36–42.
[17] N.S. McIntyre, M.G. Cook, X-ray photoelectron studies on some oxides hydroxides of cobalt, nickel, and copper, Anal. Chem. 47 (13) (1975) 2208–2213.
[18] I.G. Casella, M.R. Guascito, Anodic electrodepostion of conducting cobalt oxyhydroxide films on a gold surface. XPS study and electrochemical behaviour in neutral and alkaline solution, J. Electroanal. Chem. 476 (1999) 54–63.
[19] A. Galtayries, J. Grimblot, Formation and electronic properties of oxide and sulphide films of Co, Ni, Mo studied by XPS, J. Electron. Spectrosc. Relat. Phenom. 98–99 (1999) 267–275.
[20] N.S. McIntyre, D.D. Johnston, L.L. Coastworth, R.D. Davidson, J.R. Brown, X-ray photoelectron spectroscopic studies of thin film oxides of cobalt and molybdenum, Surf. Interface Anal. 15 (1990) 265–272.
[21] L.K. Avramon, Mechanism of CoOOH thermal decomposition, Thermochim. Acta 32 (1979) 235–239.